energy&fuels

pubs.acs.org/EF Article

Stable Carbon Isotopic Fractionation and Hydrocarbon Generation Mechanism of CO_2 Fischer–Tropsch-Type Synthesis under Hydrothermal Conditions

Zhongfeng Zhao, Qiao Feng, Hong Lu,* Pingan Peng, Tongwei Zhang, and Chang Samuel Hsu*

Cite This: *Energy Fuels* 2021, 35, 11909–11919 Read Online

ACCESS | Metrics & More | Article Recommendations

ABSTRACT: A series of gold-tube isothermal laboratory experiments at 370 °C and 50 MPa were carried out to investigate the stable carbon isotope fractionation during the formation of hydrocarbon gases from siderite reacting with the iron-bearing minerals, which simulates CO_2–H_2-rich fluids under geological settings. Only negligible amounts of hydrocarbons were generated in the pure siderite + H_2O series. However, with the addition of Fe or FeO, a large amount of methane and some amounts of C_2–C_5 gaseous hydrocarbons were produced. The generated gaseous hydrocarbons exhibit increasing $\delta^{13}C$ values with carbon number, opposite to the usual decreasing trend observed in the classical Fischer–Tropsch (FT) synthesis with CO as the carbon source. These two opposite trends in carbon isotopic distributions of hydrocarbon gases indicate different chain growth mechanisms for CO_2 versus CO as carbon sources. A carbonyl mechanism is introduced in this study to expound the rationality of the increasing trend of $\delta^{13}C$ values. Our experimental observation provides a perspective that in the Earth system where CO_2 is the main carbon source the stable carbon isotopic distributions of abiogenic hydrocarbons may display an increasing $\delta^{13}C$ distribution pattern with carbon number.

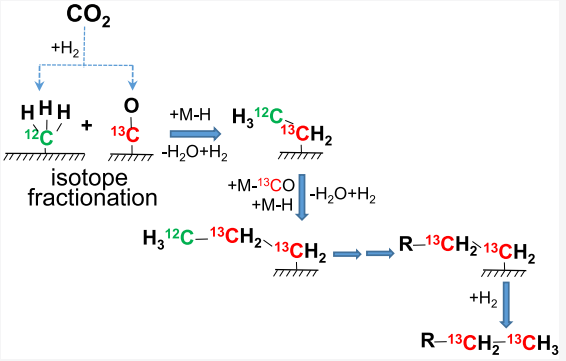

1. INTRODUCTION

Fischer–Tropsch (FT) synthesis refers to the surface-catalyzed reduction of CO by H_2 produced from natural gas, coal, or biomass in a process known as gasification. However, in the geological literature, the term Fischer–Tropsch-type (FTT) reaction is referred to as the surface-catalyzed reduction of any inorganic carbon source to generate organic compounds.[1] FTT reactions have become an important topic to understand the formation of abiotic hydrocarbons, especially in natural systems.

A lot of simulation experiments were carried out in recent years using CO and HCOOH to simulate the non-biosynthesis (abiotic synthesis) under geological conditions, resulting in high hydrocarbon yields and decreasing $\delta^{13}C$ values with carbon number ($\delta^{13}C_1 > \delta^{13}C_2 > \delta^{13}C_3 > \delta^{13}C_4$).[2,3] This was rationalized by the lighter ^{12}C to be more likely incorporated into the chain propagation based on a carbene (or carbide) mechanism of CO FT.[4−7]

However, in geological environments, CO_2 is the main source of carbon due to its relatively high chemical stability.[8] The carbon isotopic distributions of most abiogenic hydrocarbon gases in Precambrian shield and especially marine hydrothermal systems were found in an increasing $\delta^{13}C$ distribution order,[9−13] which were verified by the experimental results using CO_2 as the carbon source.[14−16] This shows that the simulation experiments with CO and HCOOH as carbon sources are not consistent with the actual hydrocarbon generation processes underground.

Siderite is a common iron-bearing mineral in Archaean,[17−19] which is precipitated in ocean through the reaction of ferrous iron with dissolved inorganic carbon anions (HCO_3^- and CO_3^{2-}) in the absence of oxygen.[20] It was also found in large amounts in microfractures in the Lafayette meteorite from Mars.[21] Thermal decomposition of siderite ($FeCO_3$) could not only provide a source for extraterrestrial organic compounds in the Martian meteorite ALH 84001[22] but also potentially form natural gas deposits within basins.[23] Unfortunately, only trace amounts of methane and other reduction products were produced in the reported simulation experiments,[22,24,25] making it difficult to obtain reliable stable carbon isotope data for genetic discrimination.

Therefore, we believe that it is necessary to conduct CO_2 simulation experiments to address the discrepancies. Siderite

Received: April 29, 2021
Revised: July 8, 2021
Published: July 23, 2021

https://doi.org/10.1021/acs.energyfuels.1c01323
Energy Fuels 2021, 35, 11909–11919

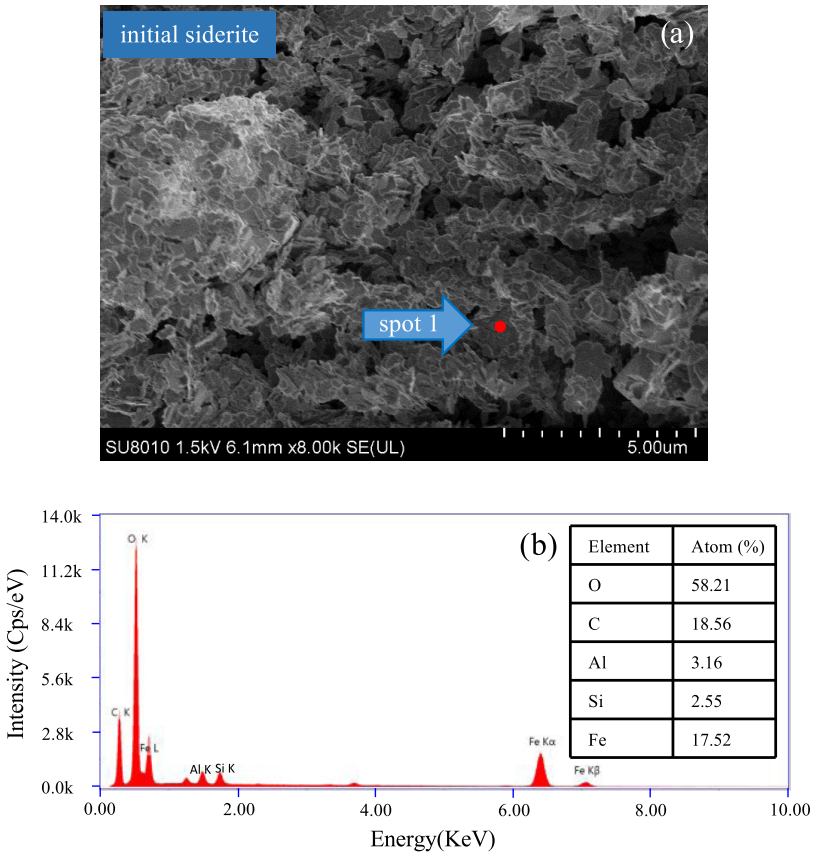

Figure 1. SEM images in the backscattered electron mode of original siderite and EDS of spot 1. Some impurities such as aluminum and silicon elements are present in siderite.

Table 1. Sample Weights Loaded in the Blank Runs (1−5) and Experiment Series (A−D), with Gas Yields in Blank Runs

code	temp. (°C)	heating time (h)	siderite (mg)	H_2O (μL)	Fe (mg)	FeO (mg)	Fe_3O_4 (mg)	CO_2[a]	H_2[a]	C_1[a]
Blk-1	370	360		50				b.d.	b.d.	b.d.
Blk-2	370	360		50	87			b.d.	15.96	b.d.
Blk-3	370	360		50		250		b.d.	15.86	b.d.
Blk-4	370	360		50			250	b.d.	b.d.	b.d.
Blk-5	370	360	60					9.15	b.d.	b.d.
series A	370	24−360	60	50						
series B	370	24−360	60	50	87					
series C	370	24−360	60	50		250				
series D	370	24−360	60	50			250			

[a]Units in μmol. [b]"b.d.", below detection.

was chosen as the carbon source because it can provide sufficient inorganic carbon and avoid the difficulties of introducing gaseous CO_2. Native iron or ferrous Fe (Fe^{II}) in the reactant minerals underground could react with water to produce H_2.[26,27] Hence, in our experiments using siderite as the carbon source, native iron or iron minerals were added to simulate the generation of abiogenic hydrocarbons under geological CO_2−H_2-rich conditions. The formation progress of hydrocarbons can then be derived from the yields of gaseous products and their stable carbon isotope fractionations.

2. EXPERIMENTS AND METHODS

2.1. Materials. Iron (Fe) and iron(II) oxide (FeO) were purchased from Alfa Aesar; the purities of them were 99 and 99.5%, respectively. Iron(II, III) oxide (magnetite, Fe_3O_4) was purchased from Sigma-Aldrich, with a purity of over 99%. Iron(II) carbonate (siderite, $FeCO_3$) was purchased from Strem Chemicals, after grinding it with a mortar and pestle; the scanning electron micrographs (SEMs) and energy-dispersive spectroscopy (EDS) are exhibited in Figure 1, which showed a scaly aggregate with a small amount of silicon and aluminum elements. Deionized water with a resistivity of about 18.8 MΩ was used in the experiments. All solid reactants were Soxhlet-extracted with dichloromethane:methanol (DCM:MeOH) (9/1, v/v) for 72 h to remove potential organic contaminants before experiments.

2.2. Experimental Methods. Experiments were conducted in flexible gold capsules (6 mm o.d., 0.25 mm wall thickness, and 60 mm length) placed within steel pressure vessels. The internal pressure in the vessels was kept stable by pumping water in or out during the experiments. The experimental apparatus has been described previously.[28] Prior to the experiments, one end of each gold tube was sealed by argon-arc welding, and then the tube was heated at 800 °C for 3 h in air to remove potential organic contaminants.

In the experiments, siderite was the initial carbon source and water was the hydrogen source. When water is used as the hydrogen source,

https://doi.org/10.1021/acs.energyfuels.1c01323
Energy Fuels 2021, 35, 11909−11919

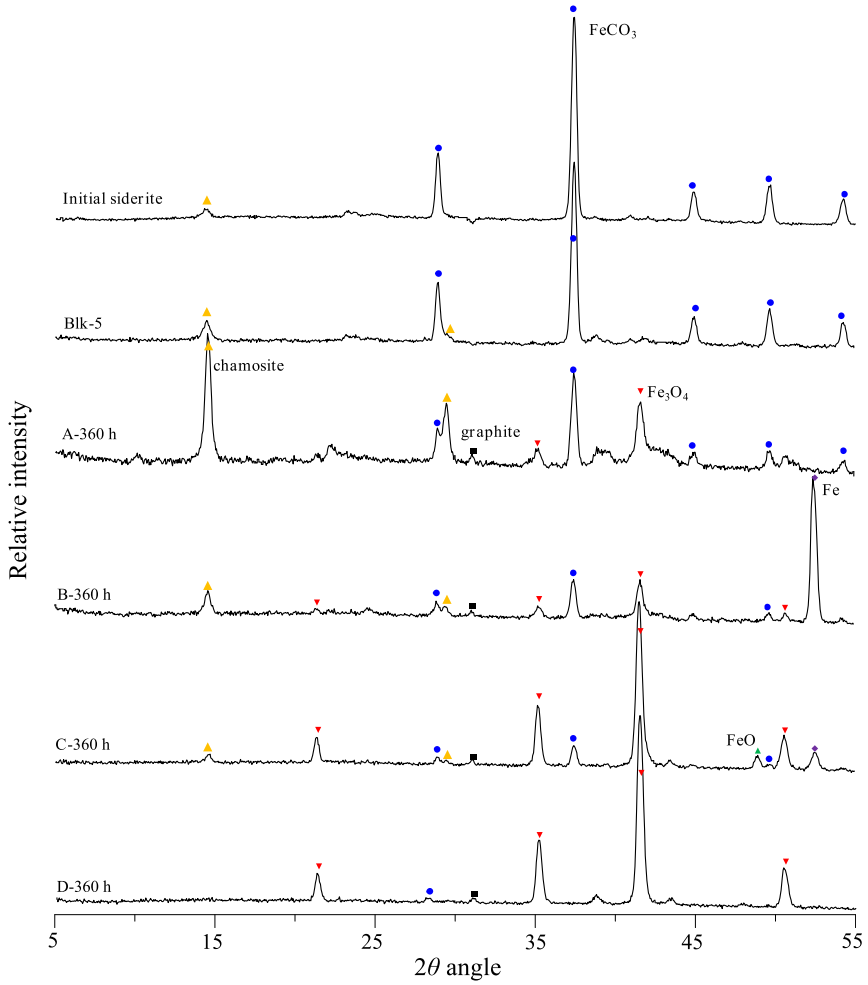

Figure 2. XRD patterns of the initial siderite and residual solids with Co-α radiation. The main peaks of the minerals were marked in each sample. Blue solid circles denote siderite, red solid down triangles denote magnetite, solid squares denote graphite, purple solid diamonds denote iron, green solid triangles denote ferrous oxide (FeO), and yellow solid triangles denote chamosite.

iron is usually used as the reducing agent in some FT experiments. The process is essentially a redox reaction, and $Fe^{(II)}$ plays the reduction role. It is believed that iron oxides have catalytic effects on abiotic hydrocarbon generation,[14,29,30] so we used Fe_3O_4 and FeO in our experiments as well. Four series of high-temperature and high-pressure thermal simulation experiments were conducted, including siderite + H_2O (series A), siderite + H_2O + Fe (series B), siderite + H_2O + FeO (series C), and siderite + H_2O + Fe_3O_4 (series D) (Table 1). According to reactions 1 and 4 shown, 2.24 mmol H_2O is needed if all siderite and Fe are exhausted. Similarly, 1.33 mmol H_2O is needed if all siderite and FeO in reactions 2 and 4 are consumed. Hence, 50 μL (2.78 mmol) of water used in series A–D (Table 1) was sufficient for the reactions.

A gap of 2 mm was left by compressing with pliers after loading the reactants, and then the tubes were placed into a cup that was filled with argon continuously for 15 min. Next, the orifice of each gold tube was clamped with pliers and the other end of the tube was immersed in cold water to ensure that, during welding, the sample would not escape or be damaged by the heating. Then, each sealed gold tube was put into water at 100 °C for leak detection (gas in the gold tubes would expand when heated, and bubbles would appear if there was gas leakage). Welded gold capsules were placed in the steel vessels, which were temperature-controlled by a computer. It has been known that Rainbow and Logatchev vent fluids of ultramafic-hosted hydrothermal vents have elevated concentrations of CO_2 and high temperatures (350–400 °C),[9] so the capsules were heated from ambient to 370 °C over a period of 10 h and then maintained at 370 °C (±1 °C) for 24, 72, 168, and 360 h. During the entire process, the vessels were maintained at an approximately constant pressure of about 50 MPa (±0.1 MPa), which is equal to the pressure of 5 km of water in depth. Water was used as the pressure control medium by an air-driven pump.[31] Each vessel containing the gold capsules was removed from the oven and quenched to room temperature in cold water within 10 min.

2.3. Analysis of Gas Components and Stable Carbon Isotopes. After the experiments, the gas components in the capsules were collected in a special glass device connected to an Agilent 6890N GC (30 m × 0.25 mm × 0.25 μm) modified by the Wasson ECE instrumentation, as described in detail elsewhere.[28] The gas collector was connected to the GC through two valves for chemical composition analysis. Once an aliquot of gas entered the GC, the valve between the gas collector and GC was closed and the remaining gas in the gas collector was kept for stable carbon isotope analysis.

Organic and inorganic gas components were analyzed simultaneously using a flame-ionization detector (FID) and a thermocouple detector (TCD). The oven temperature for hydrocarbon gas analysis was initially held at 60 °C for 3 min, ramped from 60 to 190 °C at 25 °C/min, and then held at 190 °C for 3 min. Stable carbon isotopic analysis of gaseous hydrocarbons was performed by gas chromatography-isotope ratio mass spectrometry (GC-irMS) that was coupled to a VG Isochrom II mass spectrometer with an Agilent 6890 GC using a 30 m × 0.32 mm × 0.25 μm Poraplot Q column. Helium was used as the carrier gas. The GC oven temperature was initially held at 50 °C for 3 min, ramped from 50 to 190 °C at 15 °C/min, and then held at 190 °C for 7 min. Each sample was tested at least three times

https://doi.org/10.1021/acs.energyfuels.1c01323
Energy Fuels 2021, 35, 11909–11919

Table 2. Yields of Gaseous Products and Concentrations of CO_2 and H_2 during the Simulation Experiments at 370 °C

code	time (h)	CO_2	CO	H_2	C_1	C_2	C_3	C_4	C_5	CO_2 (mol/kg)	H_2 (mmol/kg)
Siderite + H_2O (Series A)											
A-24	24	522.6		0.256	0.079	0.021	0.012	0.006	0.002	5.22	2.64
A-72	72	584.2		0.400	0.151	0.036	0.023	0.010	0.006	5.88	4.13
A-168	168	605.5		0.586	0.288	0.070	0.041	0.023	0.012	6.03	6.05
A-360	360	536.2		0.315	0.410	0.082	0.051	0.031	0.016	5.46	3.25
Siderite + H_2O + Fe (Series B)											
B-24	24	25.1	0.060	30.034	2.172	0.062	0.035	0.018	0.005	0.25	310
B-72	72	45.3	0.115	32.851	6.256	0.139	0.083	0.055	0.016	0.46	339
B-168	168	81.4	0.038	27.918	25.469	0.341	0.140	0.092	0.035	0.84	288
B-360	360	137.0	0.015	24.645	68.999	0.955	0.257	0.148	0.052	1.41	254
Siderite + H_2O + FeO (Series C)											
C-24	24		0.090	30.209	4.343	0.083	0.054	0.022	0.009		312
C-72	72		0.128	27.444	15.187	0.209	0.116	0.066	0.023		283
C-168	168	42.6	0.028	26.939	48.028	0.511	0.205	0.119	0.049	0.44	278
C-360	360	74.4	0.026	26.658	116.291	1.556	0.353	0.179	0.072	0.76	275
Siderite + H_2O + Fe_3O_4 (Series D)											
D-24	24	924.8		0.036	0.145	0.021	0.019	0.009		9.38	0.37
D-72	72	978.0		0.657	0.211	0.032	0.032	0.016		9.81	6.79
D-168	168	980.4		0.117	0.371	0.045	0.038	0.020	0.001	9.84	1.21
D-360	360	967.0		0.016	0.366	0.047	0.041	0.026	0.002	9.68	0.16

[a]Yields are expressed in mmol/mol siderite. The yields of C_2 and C_3 refer to the sum of the alkanes and alkenes, and C_4 and C_5 refer to the sum of *n*-alkanes and *i*-alkanes.

to ensure accuracy and reproducibility of $\delta^{13}C$ values to within 0.5‰ with respect to a V-PDB standard.

3. RESULTS

3.1. Blank Experiment Analysis. The control of the background carbon source is very important for abiogenic hydrocarbon generation experiments. If background organic contamination enters the experimental setup, it will compromise the results, as found in many experiments.[1,14] To ensure there were no background carbons in our studies, Soxhlet extraction was used to remove soluble organic pollutants from the reactants of siderite, iron powder, ferrous oxide, and magnetite for 72 h. Five blank experiments with the materials listed in Table 1 were carried out to evaluate the background carbon sources.

There were no carbon gases detected in blank runs, indicating that the experimental system was not contaminated. Some amounts of H_2 were obtained in the Fe+H_2O (Blk-2) and FeO + H_2O (Blk-3) runs due to reactions 1 and 2.[3,32] There was 9.15 μmol CO_2 in the Blk-5 run with 60 mg (0.52 mmol) of siderite. The $\delta^{13}C$ value of the CO_2 was −4.9‰, similar to that of siderite (−4.8‰), confirming that the CO_2 came from the decomposition of siderite

$$3Fe + 4H_2O \rightarrow Fe_3O_4 + 4H_2 \quad (1)$$

$$3FeO + H_2O \rightarrow Fe_3O_4 + H_2 \quad (2)$$

3.2. Yields of Gas Components. The gas yields of CO_2, H_2, CO, and C_1 to C_5 are discussed below:

3.2.1. [CO_2]. Studies have shown that the thermal decomposition temperature of siderite occurs between 400 and 600 °C, depending on pressure, heating rate, CO_2, and O_2 fugacities (reaction 3)[25,33,34]

$$6FeCO_3 \rightarrow 2Fe_3O_4 + 5CO_2 + C \quad (3)$$

In Blk-5, the siderite did not decompose dramatically at 370 °C, the CO_2 yield was only 9.15 μmol (Table 1), and siderite remained unchanged in the remaining solids after 360 h (Figure 2, Blk-5). However, in the siderite + H_2O series (series A), the yield of CO_2 was about 522.6 mmol/mol siderite only after 24 h. The X-ray diffraction (XRD) pattern showed that a large amount of magnetite was generated after 360 h (Figure 2, A-360 h), which indicated that water can significantly reduce the decomposition temperature and promote the cracking of siderite (reaction 4)

$$3FeCO_3 + H_2O \rightarrow Fe_3O_4 + 3CO_{2,aq} + H_{2,aq} \quad (4)$$

When iron (series B) or ferrous oxide (series C) was added, the CO_2 yield was significantly lower than that of series A (<90 mmol/mol siderite). The highest CO_2 yield (924.8−980.4 mmol/mol C) was found in the siderite + H_2O + Fe_3O_4 series (series D), whereby almost all of the siderite was decomposed (>98%) at 370 °C after heating for 360 h. The dispersed magnetite could enhance the heat conduction, making the siderite be heated evenly to promote its decomposition.

Milesi et al.[25] studied the stability domains of hematite, magnetite, wüstite, and siderite as well as the CO_2−graphite equilibrium as a function of moles of hydrogen versus moles of CO_2 in water at 300 °C and 50 MPa, close to our experimental conditions. Compared to the reported results of the saturation concentrations of H_2 (>1.67 mol/L) and CO_2 (>10 mol/L) under 300−350 °C and 30−50 MPa,[25,35] our H_2 and CO_2 concentrations were less than their values, especially for H_2 (Table 2). Hence, their plot of log $m_{H2(aq)}$ versus log $m_{CO2(aq)}$, where $m_{H2(aq)}$ and $m_{CO2(aq)}$ stand for the mole of H_2 or CO_2 per kilogram of water, respectively, was used in our studies.

There is an equilibrium between H_2 and CO_2 in water in the presence of siderite and magnetite, shown in eq 4. We entered our data of series A−D listed in Table 2 into the log $m_{H2(aq)}$ vs log $m_{CO2(aq)}$ plot of Milesi et al., shown in Figure 3, with some modifications for 370 °C.

All series were close to the siderite−magnetite equilibrium, especially for series A where only siderite was added with water. All other series with additional iron and its minerals

https://doi.org/10.1021/acs.energyfuels.1c01323
Energy Fuels 2021, 35, 11909−11919

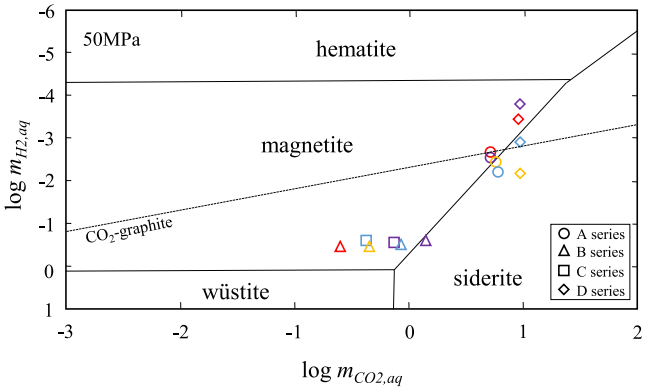

Figure 3. Modified phase diagram for stability domains of hematite, magnetite, wüstite, and siderite as well as the CO_2−graphite equilibrium at 50 MPa and 370 °C based on Milesi et al.[25] The colors in red, orange, blue, and purple refer to the heating time of 24, 72, 168, and 300 h, respectively.

showed slight deviations. Series B and C approached equilibrium with longer heating times (moving to the right toward equilibrium). However, the vertical spread in series D was due to the tiny amounts of H_2 being measured (Table 2). The presence of graphite in all four series (Figure 2) indicated that the magnetite−siderite−graphite mineral assemblage buffered the CO_2−H_2 concentrations.

3.2.2. [H_2]. Trace amounts of hydrogen gas were generated in series A (0.3−0.6 mmol/mol C). The H_2 yields in series D (0.0−0.7 mmol/mol) were close to that in series A, indicating that the $Fe^{(II)}$ in magnetite was not effective to exchange the H atom in water to form hydrogen gas. In series B and C, the presence of elemental iron (Fe) and ferrous oxide (FeO) as catalysts greatly enhanced hydrogen gas generation. A large amount of hydrogen gas was present in series B (24.6−32.9 mmol/mol C) and C (26.6−30.2 mmol/mol C) than in series D (Table 2).

The process in series B can be attributed to electron transfer from Fe^0 (reaction 1),[30] while in series C, it can be attributed to a redox reaction of FeO (reaction 2).[30] Electrons in Fe^0 and FeO can transfer to hydrogen (proton) in water, thus producing H_2. The H_2 yields did not change significantly over time. The XRD results of the 360 h samples in series B and C showed some siderite and Fe/FeO residues (Figure 2B,C, 360 h), indicating sufficient amounts of Fe and FeO remaining to function as catalysts after generating hydrogen (reactions 1 and 2).

3.2.3. [CO]. With the high yields of H_2, some amounts of CO (0.015−0.128 mmol/mol C) were found in series B and C. It could be generated by the reverse water gas shift (RWGS) reaction[3] (reaction 5), but the contents of CO were much lower than that of CO_2. The contents of CO in the two series decreased gradually after 72 h

$$CO_2 + H_2 \leftrightarrow CO + H_2O \quad (5)$$

On the one hand, CO could form hydrocarbons through the FT reaction (reaction 6); on the other hand, CO could also go through the disproportionation reaction to produce CO_2 and graphitic carbon[33] (reaction 7)

$$CO + H_2 \rightarrow CH_4 + H_2O \quad (6)$$

$$2CO \rightarrow C + CO_2 \quad (7)$$

3.2.4. [C_1−C_5]. Trace amounts of methane (<1 mmol/mol) were generated in series A and D (Figure 4), which were consistent with the experimental results of Milesi et al.[25] In addition, the yields of C_2−C_5 were 1 or 2 orders of magnitude less than methane. The gaseous hydrocarbons in series A and D were formed by the reduction of inorganic carbon according to reaction 8.[36−38] When the H_2/CO_2 ratio was relatively low, the ability to form reduced carbon was limited,[14] and the conversion to reduced carbons (gaseous hydrocarbons) was less than 1%. The yields of gaseous hydrocarbons increased significantly in series B and C with added native Fe and FeO,

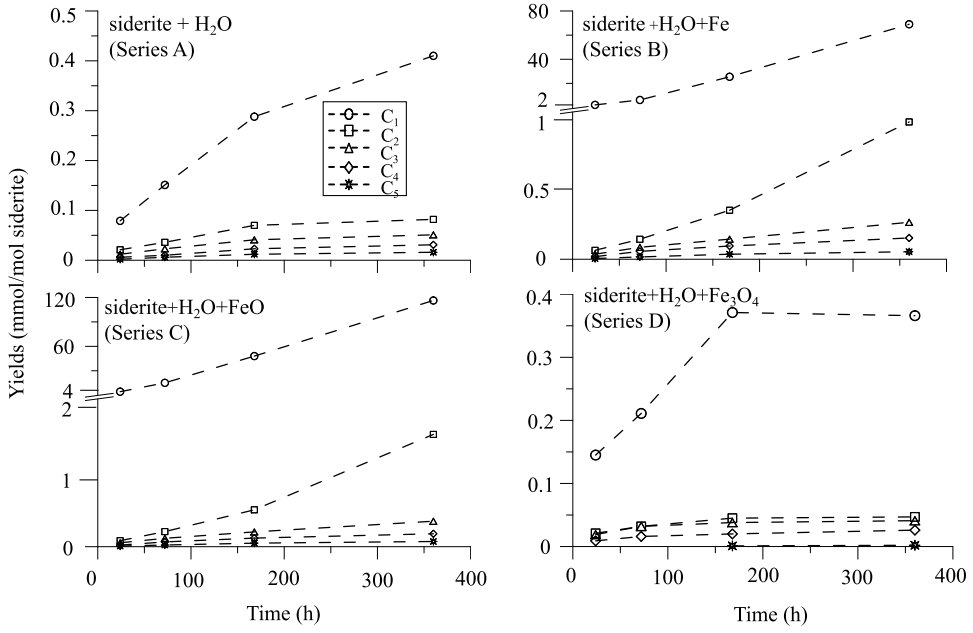

Figure 4. Yields of C_1−C_5 hydrocarbons in four series of siderite experiments. The yields of C_2 and C_3 refer to the sum of the alkanes and alkenes, and C_4 and C_5 refer to the sum of *n*-alkanes and *i*-alkanes.

https://doi.org/10.1021/acs.energyfuels.1c01323
Energy Fuels 2021, 35, 11909−11919

respectively. The amounts of methane were 2−3 orders of magnitude higher than those of C_2−C_5, and the yields of hydrocarbon gases kept increasing with time. These indicate that the gaseous hydrocarbons were derived from the abiogenic processes

$$CO_2 + 4H_2 \rightarrow CH_4 + 2H_2O \quad (8)$$

3.3. Stable Carbon Isotopic Compositions of the Gaseous Products. The stable carbon isotopic compositions of the gaseous products are shown in Table 3. In series A and D, the $\delta^{13}C$ values of CO_2 were about −5 ± 1‰ with almost no carbon isotope fractionations, compared with the initial $\delta^{13}C$ value of siderite (−4.8‰). However, in series B and C, CO_2 gradually became heavier from 24 h (−9.8 and −8.7‰) to 360 h (+1.2 and −0.8‰). It is worth noting that CO in series B and C was lighter than CO_2 and gradually became heavier from 24 h (−30.8 and −38.5‰) to 360 h (−15.7 and −14.7‰).

Table 3. Stable Carbon Isotopic Compositions of Gaseous Products in the Simulation Experiments on Siderite at 370 °C (All $\delta^{13}C$ Values Are in ‰)

code	time (h)	$\delta^{13}C$ CO_2	$\delta^{13}C$ CO	$\delta^{13}C$ CH_4	$\delta^{13}C$ C_2H_6	$\delta^{13}C$ C_3H_8	$\delta^{13}C$ n-C_4H_{10}
Siderite + H_2O (Series A)							
A-24	24	−4.8					
A-72	72	−5.0					
A-168	168	−4.8					
A-360	360	−5.0					
Siderite + H_2O + Fe (Series B)							
B-24	24	−9.8	−30.8	−38.4	−27.8	−25.6	
B-72	72	−8.4	−28.9	−43.7	−30.3	−26.8	−24.6
B-168	168	−6.5	−21.0	−46.2	−34.2	−27.0	−24.2
B-360	360	1.2	−15.7	−40.0	−34.3	−26.9	−24.5
Siderite + H_2O + FeO (Series C)							
C-24	24	−8.7	−38.5	−45.2	−33.0	−25.9	
C-72	72	−7.5	−35.6	−41.7	−33.7	−26.6	−25.9
C-168	168	−5.6	−22.6	−39.6	−34.1	−27.0	−25.5
C-360	360	−0.8	−14.7	−37.6	−34.7	−27.7	−25.2
Siderite + H_2O + Fe_3O_4 (Series D)							
D-24	24	−5.0					
D-72	72	−6.0					
D-168	168	−5.8					
D-360	360	−5.5					

The $\delta^{13}C_{C1}$ values in series B were −38.4‰ at 24 h, −46.2‰ at 168 h, and −40.0‰ at 360 h. The $\delta^{13}C_{C2}$ values gradually decreased from 24 h (−27.8‰) to 168 h (−34.2‰) and then with no further changes. The $\delta^{13}C_{C1}$ values in series C increased from 24 h (−45.2‰) to 360 h (−37.6‰), with no significant changes in the $\delta^{13}C_{C2}$ values all the time. In each series, the $\delta^{13}C_{C1}$ value was lowest, and the values increased with increasing carbon number (Figure 5).

The $\delta^{13}C$ values of the gaseous hydrocarbons, carbon monoxide, and carbon dioxide <168 h in series B and C were all less (lighter) than that of the original siderite (Table 3) because many solid coproducts, such as carbides and graphite,[37] were enriched with ^{13}C.[26] This can explain the ^{13}C depletion in all gaseous hydrocarbons.

4. DISCUSSION

4.1. Mass Balance. In the siderite + H_2O series, the yields of CO_2 were about 500−600 mmol/mol siderite. According to reaction 4, there should have been 1 mole of H_2 produced for every 3 moles of CO_2, which means that the stoichiometric yields of H_2 should be about 167 mmol/mol siderite in this series. Yet, barely any H_2 was observed in the experiments (<1 mmol/mol siderite; Table 2). Some possible reasons for this situation include the following: (1) The ratio of CO_2:H_2 in our experiments was in agreement with that of Milesi et al.;[25] both were more than 100:1 and quite different from the stoichiometric value of 3:1. The authors believe that the formation of condensed carbon contributed another path to consume H_2 (reaction 9), which was confirmed by the presence of a graphite peak in XRD (Figure 2). (2) The siderite contained impurities of Si and Al (Figure 1b), resulting in the combination of the silica−alumina mineral with $Fe^{(II)}$ in siderite to form the aluminosilicate mineral of chamosite ($Fe_x[(Si, Al)_4O_{10}](OH)_8$ that was rich in $Fe^{(II)}$ (Figure 2). So, the Fe^{2+} would be fixed as chamosite, resulting in a low H_2 yield. (3) There were iron and FeO residues in series B and C, and the H_2 yields reached the maximum within 24 h. These facts indicated that reactions 1 and 2 were fast and quickly reached equilibrium. Besides, some H_2 reacted with CO_2 to form hydrocarbons (reaction 8). In brief, H_2 generation by reactions 1 and 2 quickly reached an equilibrium, accompanied by partial consumption of the generated H_2 by reactions 8 and 9. Hence, a low H_2 yield in our system seems to be reasonable

$$CO_2 + 2H_2 \rightarrow C + 2H_2O \quad (9)$$

The presence of significant amounts of siderite in A-360 h of Figure 2 indicated that siderite was not decomposed completely after 360 h. According to thermodynamic calculations by Milesi et al.,[25] the experimental system would reach the overall equilibrium of magnetite−wüstite−siderite,

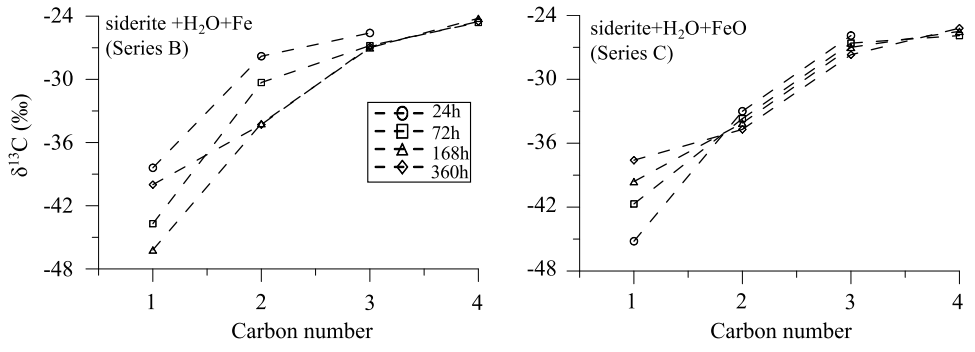

Figure 5. $\delta^{13}C$ values of hydrocarbon species (C_1−C_4) with carbon numbers in siderite experiments.

https://doi.org/10.1021/acs.energyfuels.1c01323
Energy Fuels 2021, 35, 11909−11919

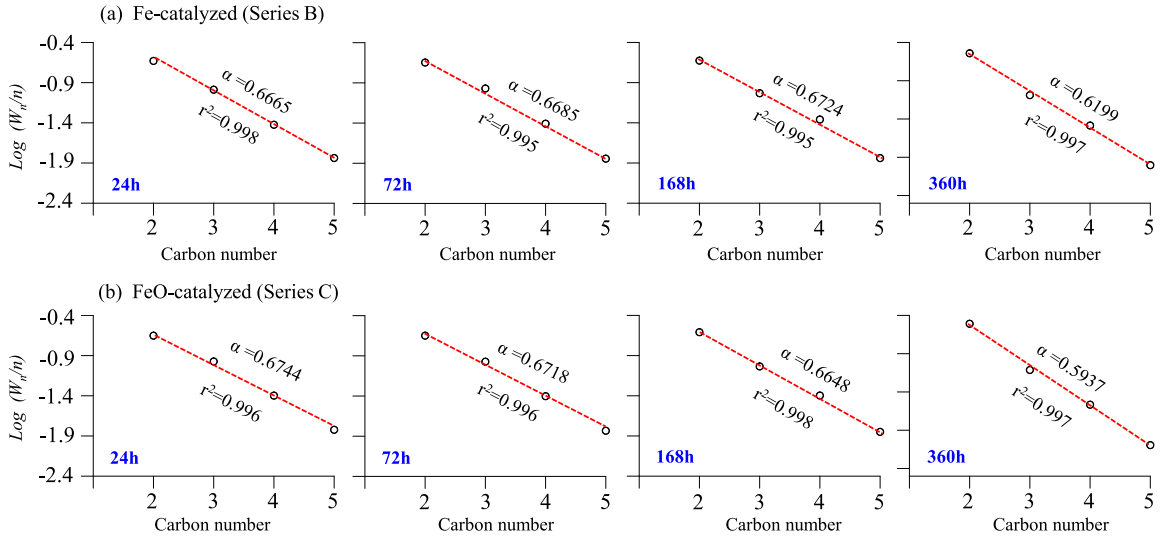

Figure 6. Anderson–Schulz–Flory distributions of C_2–C_5 in series B and C. Note that all of the correlation coefficients r^2 exceed 0.99, which indicate an abiotic source by the FTT synthesis.

Table 4. Stable Carbon Isotopic Values ($\delta^{13}C$, ‰) of Gaseous Products in Some Abiogenic Hydrocarbon Experiments from Literatures

carbon source	catalyst	t (°C)/P (MPa)	Time (h)	$\delta^{13}C$ (CH_4)	$\delta^{13}C$ (C_2H_6)	$\delta^{13}C$ (C_3H_8)	$\delta^{13}C$ (C_4H_{10})	ref
CO	Fe + zeolite	296/3	20	−39.4	−44.7	−46.1	−48.7	45
	Fe + zeolite	296/3	40	−43.3	−42.6	−44.4	−44.6	45
	Fe + Co + zeolite	308/3	90	−49.6	−42.0	−45.3	−46.4	45
	Fe_3O_4	280/0.7	4	−51.2	−33.0	−49.8	−52.2	2
	Fe	252/17	2.75	−60.3	−50.7	−52.9	−56.0	3
	Fe	252/17	18	−60.2	−53.7	−54.0	−56.0	3
CO_2	Fe	350/10	12	−69.9	−68.2	−66.8	−66.1	16
	Co	245/10	9	−79.6	−76.3	−75.6		16
	K-10 + Fe^{3+} + Ni^{3+}	400/50	5	−31.9	−27.6	−26.4	−25.5	31
	K-10 + Fe^{3+} + Ni^{3+}	400/50	20	−44.5	−34.3	−30.5	−28.1	31
	Fe_3O_4	400/50	510	−33.5	−28.0	−25.7		14
	Fe_3O_4	400/50	1015	−39.2	−25.8	−23.7		14

[a]Note: dashes denote no data.

CO_2, and graphite. Based on our data of the CO_2 yields and residual siderite, the equilibrium was reached quickly in the early stage of the experiments. The large amounts of H_2 in series B and C may inhibit the decomposition of siderite (reaction 4), resulting in siderite remaining as a main carbon-containing substance. However, the XRD peak heights of siderite in series B and C (Figure 2B,C, 360 h) were significantly lower than that in series A (Figure 2A, 360 h) due to the dilution by large amounts of Fe and FeO being added. Lower yields of CO_2 were obtained in series B and C relative to that of series A because of much more H_2 being present in series B and C to accelerate reaction 9, resulting in more graphite carbon and hydrocarbon gases formed. Therefore, the carbon could maintain mass balance and mainly existed in the forms of siderite, graphitic, hydrocarbons, and CO_2.

4.2. Abiogenic Gaseous Hydrocarbon Yields and Increasing $\delta^{13}C$ Values with Carbon Number. A number of studies have shown that the hydrocarbon products obtained from the Fischer–Tropsch synthesis follow the Anderson–Schulz–Flory (ASF) distribution[39,40] (eq 10)

$$W_n/n = (1-\alpha)^2 . \alpha^{n-1} \quad (10)$$

where n is the number of carbon atoms in the products, w is the weight fraction of products containing n carbon atoms, and α is the probability of chain growth. Etiope et al.[41] tested the Anderson–Schulz–Flory distributions on selected thermogenic gas samples and presumed abiotic gas samples from natural sources. They considered that a correlation coefficient (r^2) of >0.9 (eq 10) may indicate a dominant abiotic component, with (r^2) > 0.99 likely referring to almost pure abiotic gases.

However, the yields of CH_4 were always consistently in excess of C_2H_6 and C_3H_8 in many other experiments, especially when CO_2 was used as the reactant,[14,16,31] because the weak affinity of CO_2 adsorption on a catalyst surface may result in a low C/H ratio at catalytic sites, favoring methane formation and inhibiting the chain growth probability.[42] Methane yields were much higher than long-chain gaseous hydrocarbons in series B and C (Table 2 and Figure 4). According to eq 10, C_2–C_5 in the two series fitted the Anderson–Schulz–Flory distribution perfectly (Figure 6), indicating the FTT products, and the excess methane may also come from CO_2 methanation, such as the Sabatier reaction (reaction 8). This reaction reduces CO_2 to methane only,[43] which is considered to be an important source of methane in the Martian

https://doi.org/10.1021/acs.energyfuels.1c01323
Energy Fuels 2021, 35, 11909–11919

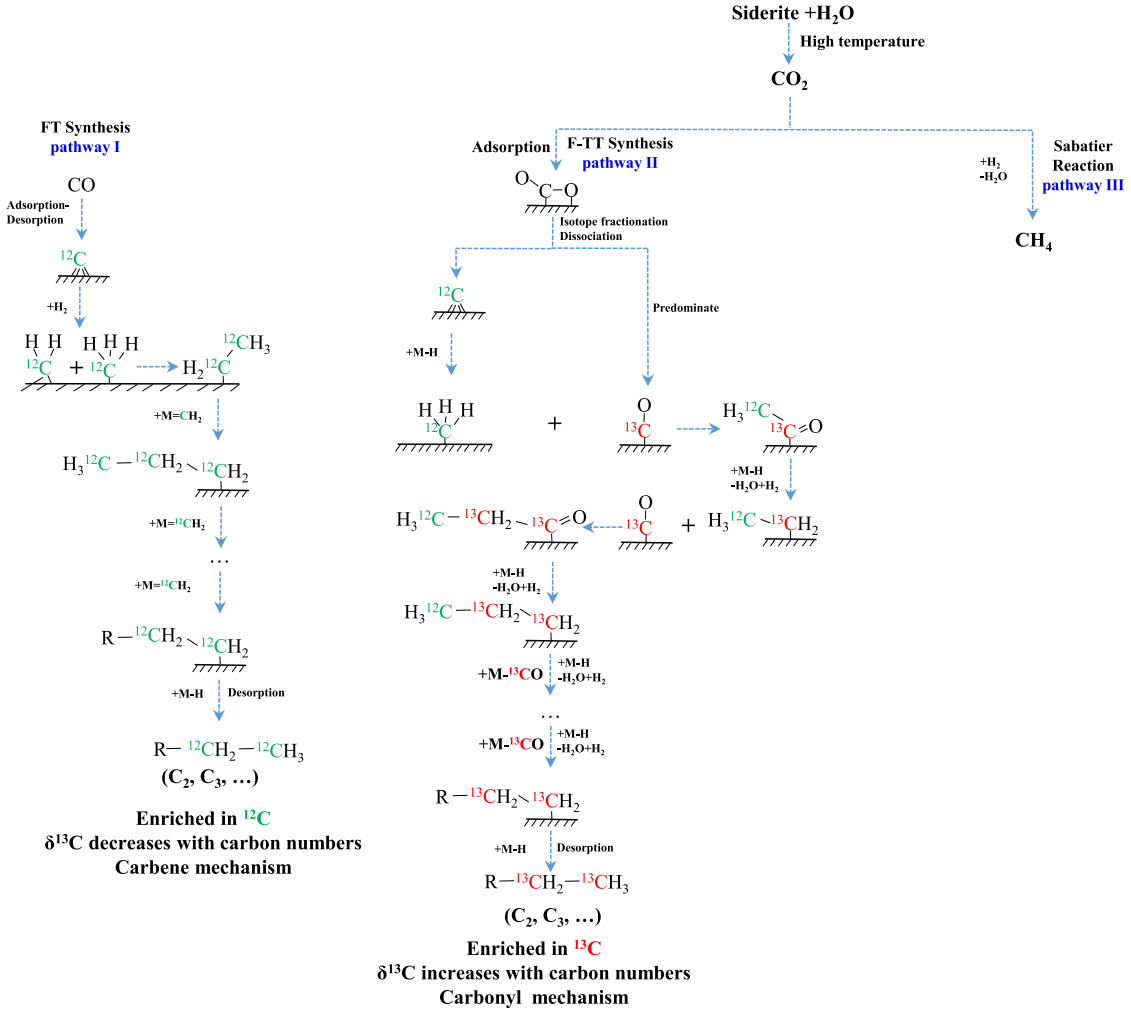

Figure 7. Abiotic hydrocarbon generation mechanisms and stable carbon isotopic fractionation.

atmosphere.[44,45] Therefore, it is necessary to separate methane from C_2-C_5 in the following isotope discussions.

In recent years, a lot of simulation experiments on abiotic hydrocarbon generation with CO and CO_2 as carbon sources have been conducted under different experimental conditions, as summarized in Table 4. The results showed that when CO was the carbon source, the carbon isotope distribution of C_2-C_4 was generally in a decreasing order ($\delta^{13}C_2 > \delta^{13}C_3 > \delta^{13}C_4$) (Table 4).[2,3,46] Methane is not considered here because of its genetic complexity that can interfere the distributions of carbon isotopes. In our experiments, the carbon isotopes of gaseous hydrocarbons were heavier than that of CO, which clearly indicated that C_2-C_4 did not come from the FT reaction by CO. When CO_2 was the carbon source, the carbon isotope distribution of C_2-C_4 generally showed an increasing order ($\delta^{13}C_2 < \delta^{13}C_3 < \delta^{13}C_4$).[14−16] The ^{13}C isotope distributions of gaseous hydrocarbons in series B and C with siderite as the carbon source were also in an increasing trend ($\delta^{13}C_2 < \delta^{13}C_3 < \delta^{13}C_4$). Besides, $\Delta(\delta^{13}C_{CO} - \delta^{13}C_{CnH2n+2,n>1})$ > 30−40‰,[3,46] compared to −15−20 in Table 3, confirming that C_2-C_4 in our experiments did not come from the FT reaction by CO. These observations suggest that the reaction mechanisms of Fischer−Tropsch-type reactions with CO and CO_2 as the carbon sources are quite different, which might be the main cause of the $\delta^{13}C$ distribution characteristics in our siderite experiment.

4.3. Abiotic Hydrocarbon Generation and Carbon Isotope Fractionation. There are essentially two generally accepted mechanisms, shown in Figure 7, for the stepwise chain growth in FT reactions.[47,48] One is the "carbene mechanism" (pathway I), where the metal-bonded carbon (carbide) from (M−CO) is followed by $M-CH_2$ as the basic unit species for the carbon chain growth. Since $M-^{12}CH_2$ reacts faster than $M-^{13}CH_2$, the lighter species is more likely to be incorporated into larger hydrocarbon chains.[4,5] This mechanism has been used to explain the decreasing $\delta^{13}C$ value characteristics of hydrocarbons via FT synthesis with CO as the carbon source. Another mechanism is the "carbonyl mechanism" (pathway II), where the chain growth is proceeded by a surface-bonded carbonyl (M−CO) followed by hydrogenation−dehydration−hydrogenation to form hydrocarbons eventually,[49] as discussed below for CO_2 FTT.

In the case of the dissociative adsorption of CO_2, the process can proceed as reaction 11[16]

$$CO_2 \rightarrow x(M-CO) + y(M-C) + z(M-O) + w(M-CO_2) \quad (11)$$

The alkyl chain generation and carbon isotope fractionation formed by CO_2 are shown as pathway II in Figure 7. Because the $O-^{12}C-O$ is more reactive than the $O-^{13}C-O$, M−CO and M−C are depleted in ^{13}C than the initial CO_2.[16] Furthermore, $M-^{12}C$ is easier to be connected to the H

https://doi.org/10.1021/acs.energyfuels.1c01323
Energy Fuels 2021, 35, 11909−11919

Table 5. Stable Carbon Isotopic Values ($\delta^{13}C$, ‰) of Gaseous Products with Abiogenic Hydrocarbon Generation in Natural Environments

	location	sample	$\delta^{13}C$ (CH_4)	$\delta^{13}C$ (C_2H_6)	$\delta^{13}C$ (C_3H_8)	$\delta^{13}C$ (C_4H_{10})	ref
precambrian shields	Precambrian Shield (Canada)	CCS4546	−32.0	−34.6	−33.4		12
		8428	−34.0	−36.4	−34.9	−34.4	13
		8558	−32.7	−36.8	−35.3	−34.8	13
	Precambrian Shield (South Africa)	DR548	−46.5	−50.5	−47.2	−45.6	12
		KL443HWDN	−34.3	−34.3	−33.5		13
		KL739	−28.7	−30.7	−27.2		12
		KL441H3	−40.0	−30.9	−25.2		12
submarine hydrothermal fields	Rainbow	Exo-D7-Ti1	−17.7	−13.7	−13.0		10
		Exo-D9-Ti4	−17.8	−13.4	−13.0		10
	Lost City	H05-IGT7	−11.8	−13.7	−13.4		9
		H03-IGT7	−11.8	−14.3	−14.0		9
	Logatchev	SE-DV7-Ti3-L1	−10.3	−13.0	−8.0		10
	Von Damm	J2-612-IGT2	−15.6	−12.2	−9.8		51
		J2-617-IGT6	−15.8	−13.2	−10.8		51
		J2-621-IGT2	−15.1	−12.9	−9.7		51

atom than M−^{13}C, causing M−CH_3 to be more depleted in ^{13}C than M−CO. M−CO can be further dissociated to form M−C on the metal surface, resulting in M−C being heavier than M−CO. At the same time, M−^{12}CO is easier to cleave from the metal surface than M−^{13}CO and it no longer participated in the FTT reactions.

Once the M−$^{12}CH_3$ is generated on the metal surface, the subsequent incorporation with M−^{13}CO remaining on the metal surface increases the carbon number of the growing chain,[48] followed by hydrogenation (to hydroxy)−dehydration (to alkenyl)−hydrogenation (to alkyl) to form M−$^{13}CH_2{}^{12}CH_3$ as a growing chain. The metal-bonded alkyl can further incorporate with another M−^{13}CO to make the hydrocarbon chain even longer (Figure 7, pathway II). After each incorporation step, the carbon−metal bond can be cleaved from the metal surface in the presence of H_2 to release C_nH_{2n+2}. Because the M−CO inserted into the growing alkyl chain is gradually enriched with ^{13}C, the carbon isotope composition of the resulting alkanes becomes heavier.

In our experiments, methane can come from CO_2 methanation, such as the Sabatier reaction. There are three conceivable pathways toward methane synthesis, including the carbide pathway, formate pathway, and carboxyl pathway.[11] In these three reaction paths, CO_2 undergoes multistep reduction reactions and finally realizes methanation. ^{12}C is more reactive than ^{13}C in the process (because the O═^{12}C═O bond is weaker than the O═^{13}C═O one) to produce methane, so carbon isotopes of the residual CO_2 become heavier gradually.

4.4. Implications for Abiogenic Gas in Natural Systems. Hydrocarbon generation of siderite in the hydrogen-rich fluid may have implications not only for the abiogenic methane in the atmosphere of Mars but also for the evolution of prebiotic organic molecules in the early Earth. Therefore, the study of abiogenic hydrocarbon characteristics is worthy of attention.

In geological environments, CO_2 is the main source of carbon.[8] The carbon isotopic distributions of abiogenic hydrocarbons in the Precambrian shield and marine hydrothermal systems are summarized in Table 5; it can be seen that the $\delta^{13}C_{(C2-C4)}$ values of the abiogenic hydrocarbons often showed an increasing order. For example, $\delta^{13}C_2 < \delta^{13}C_3$ was found in the Precambrian shield in the Driefontein/Kloof areas of South Africa and the Copper Cliff area of Canada;[12] carbon isotopes of the Precambrian shield gas in the Kidd Creek area of Canada showed that the $\delta^{13}C_2$ value was lowest and then gradually increased with the carbon number ($\delta^{13}C_2 < \delta^{13}C_3 < \delta^{13}C_4$).[13] The carbon isotopes of abiogenic hydrocarbons in the marine hydrothermal systems also showed an increasing $\delta^{13}C$ trend with carbon number, but the $\delta^{13}C_{C1-C3}$ values were much greater than that in the Precambrian shield, which might be related to the different reaction conditions.[50] These indicate that in many geochemistry papers the carbon isotope distributions of hydrocarbon gases generated by CO_2 FTT reactions in geological settings may have been mistakenly rationalized based on the CO FT mechanisms. The increasing $\delta^{13}C$ trend expounded in our studies based on the generation mechanisms could be helpful for the understanding of FTT in geological environments.

5. CONCLUSIONS

Our simulation experiments under 370 °C showed that CO_2 derived from siderite pyrolysis can be catalytically reduced to gaseous hydrocarbons under hydrogen-rich fluid conditions. In the gaseous hydrocarbon products, the dominated methane was mostly from CO_2 methanation (such as the Sabatier reaction), and C_2-C_5 were generated by FTT reactions. However, the $\delta^{13}C$ values of C_2-C_5 increased with carbon numbers ($\delta^{13}C_1 < \delta^{13}C_2 < \delta^{13}C_3 < \delta^{13}C_4$), which have also been verified by simulation experiments and geological case studies in the literature. This kind of $\delta^{13}C$ carbon isotope distribution characteristic was obviously opposite to the decreasing $\delta^{13}C$ values with the carbon number of abiogenic hydrocarbons produced in the classical FT synthesis with CO as the carbon source. Thus, we introduced a carbonyl mechanism to explain the increasing $\delta^{13}C$ order in C_{2+} hydrocarbons via CO_2 FTT reactions. In the end, we believe that the carbon isotopes of most abiogenic hydrocarbons generated with CO_2 as the carbon source in the Earth system would be in the increasing $\delta^{13}C$ rather than decreasing $\delta^{13}C$ trend with carbon number as in the FT synthesis with CO as the carbon source.

AUTHOR INFORMATION

Corresponding Authors

Hong Lu − *State Key Laboratory of Organic Geochemistry, Guangzhou Institute of Geochemistry, Chinese Academy of*

https://doi.org/10.1021/acs.energyfuels.1c01323
Energy Fuels 2021, 35, 11909−11919

Sciences, Guangzhou 510640, China; CAS Center for Excellence in Deep Earth Science, Guangzhou 510640, China; Email: luhong@gig.ac.cn

Chang Samuel Hsu − *Petro Bio Oil Consulting, Tallahassee, Florida 32312, United States; Department of Chemical and Biomedical Engineering, Florida A & M University/Florida State University, Tallahassee, Florida 32310, United States; State Key Laboratory of Heavy Oil Processing, China University of Petroleum, Beijing 102249, China*; orcid.org/0000-0003-4411-7860; Email: chsu@eng.famu.fsu.edu

Authors

Zhongfeng Zhao − *State Key Laboratory of Organic Geochemistry, Guangzhou Institute of Geochemistry, Chinese Academy of Sciences, Guangzhou 510640, China; CAS Center for Excellence in Deep Earth Science, Guangzhou 510640, China; University of Chinese Academy of Sciences, Beijing 100049, China*

Qiao Feng − *Shandong Provincial Key Laboratory of Depositional Mineralization and Sedimentary Minerals, Shandong University of Science and Technology, Qingdao 266000, China*

Pingan Peng − *State Key Laboratory of Organic Geochemistry, Guangzhou Institute of Geochemistry, Chinese Academy of Sciences, Guangzhou 510640, China; CAS Center for Excellence in Deep Earth Science, Guangzhou 510640, China*

Tongwei Zhang − *Bureau of Economic Geology, The University of Texas at Austin, Austin, Texas 78713, United States*

Complete contact information is available at: https://pubs.acs.org/10.1021/acs.energyfuels.1c01323

Notes

The authors declare no competing financial interest.

■ ACKNOWLEDGMENTS

This work was supported by the National Key R & D Program of China (No. 2017YFC0603102) and also partially supported by the Strategic Priority Research Program of the Chinese Academy of Sciences (No. XDA14010102) and Chinese NSF grants (Nos. 41973069 and 41673045). The authors also thank Dr. Q. Wang for his technical assistance with GC and GC-irMS analyses. This is contribution No.IS-3049 from GIGCAS.

■ REFERENCES

(1) McCollom, T. M. Laboratory Simulations of Abiotic Hydrocarbon Formation in Earth's Deep Subsurface. *Rev. Mineral. Geochem.* **2013**, *75*, 467−494.

(2) Hu, G. X.; Ouyang, Z. Y.; Wang, X. B.; Wen, Q. B. Carbon isotopic fractionation in the process of Fisher−Tropsch reaction in primitive solar nebula. *Sci. China, Ser. D: Earth Sci.* **1998**, *41*, 202−207.

(3) McCollom, T. M.; Sherwood Lollar, B.; Couloume, G. L.; Seewald, J. S. The influence of carbon source on abiotic organic synthesis and carbon isotope fractionation under hydrothermal conditions. *Geochim. Cosmochim. Acta* **2010**, *74*, 2717−2740.

(4) Des Marais, D. J.; Donchin, J. H.; Nehring, N. L.; Truesdell, A. H. Molecular carbon isotopic evidence for the origin of geothermal hydrocarbons. *Nature* **1981**, *292*, 826−828.

(5) Sherwood Lollar, B.; Westgate, T. D.; Ward, J. A.; Slater, G. F.; Lacrampe-Couloume, G. Abiogenic formation of alkanes in the Earth's crust as a minor source for global hydrocarbon reservoirs. *Nature* **2002**, *416*, 522−524.

(6) Lancet, S. M.; Anders, E. Carbon isotope fractionation in the Fischer-Tropsch synthesis and in meteorites. *Nature* **1970**, *170*, 980−982.

(7) Yuen, G.; Blair, N.; Des Marais, D. J.; Chang, S. Carbon isotope composition of low molecular weight hydrocarbons and monocarboxylic acids from Murchison meteorite. *Nature* **1984**, *307*, 252−254.

(8) Glasby, G. P. Abiogenic Origin of Hydrocarbons: An Historical Overview. *Resour. Geol.* **2006**, *56*, 83−96.

(9) Proskurowski, G.; Lilley, M. D.; Seewald, J. S.; Früh-Green, G. L.; Olson, E. J.; Lupton, J. E.; Sylva, S. P.; Kelley, D. S. Abiogenic hydrocarbon production at Lost City hydrothermal field. *Science* **2008**, *319*, 604−607.

(10) Charlou, J. L.; Donval, J. P.; Konn, C.; Ondréas, H.; Fouquet, Y.; et al. High production and fluxes of H_2 and CH_4 and evidence of abiotic hydrocarbon synthesis by serpentinization in ultramafic-hosted hydrothermal systems on the Mid-Atlantic Ridge. *Geophys. Monogr. Ser.* **2010**, *188*, 265−296.

(11) Vogt, C.; Monai, M.; Kramer, G. J.; Weckhuysen, B. M. The renaissance of the Sabatier reaction and its applications on Earth and in space. *Nat. Catal.* **2019**, *2*, 188−197.

(12) Sherwood Lollar, B.; Lacrampe-Couloume, G.; Slater, F.; Ward, J.; Moser, D. P.; Gihring, T. M.; Lin, L. H.; Onstott, T. C. Unravelling abiogenic and biogenic sources of methane in the Earth's deep subsurface. *Chem. Geol.* **2006**, *226*, 328−339.

(13) Lollar, B. S.; Lacrampe-Couloume, G.; Voglesonger, K.; Onstott, T. C.; Pratt, L. M.; Slater, G. F. Isotopic signatures of CH_4 and higher hydrocarbon gases from Precambrian Shield sites: a model for abiogenic polymerization of hydrocarbons. *Geochim. Cosmochim. Acta* **2008**, *72*, 4778−4795.

(14) Fu, Q.; Sherwood Lollar, B.; Horita, J.; Couloume, J. L.; Seyfried, W. E., Jr. Abiogenic formation of hydrocarbons under hydrothermal conditions: constraints from chemical and isotopic data. *Geochim. Cosmochim. Acta* **2007**, *71*, 1982−1998.

(15) Fu, Q.; Socki, R. A.; Niles, P. B. Evaluating reaction pathways of hydrothermal abiotic organic synthesis at elevated temperatures and pressures using carbon isotopes. *Geochim. Cosmochim. Acta* **2015**, *154*, 1−17.

(16) Taran, Y. A.; Kliger, G. A.; Cienfuegos, E.; Shuykin, A. N. Carbon and hydrogen isotopic compositions of products of open-system catalytic hydrogenation of CO_2: implications for abiogenic hydrocarbons in Earth's crust. *Geochim. Cosmochim. Acta* **2010**, *74*, 6112−6125.

(17) van Zuilen, M. A.; Lepland, A.; Teranes, J.; Finarelli, J.; Wahlen, M.; Arrhenius, G. Graphite and carbonates in the 3.8 Ga old Isua Supracrustal Belt, southern West Greenland. *Precambrian Res.* **2003**, *126*, 331−348.

(18) Hessler, A. M.; Lowe, D. R.; Jones, R. L.; Bird, D. K. A lower limit for atmospheric carbon dioxide levels 3.2 billion years ago. *Nature* **2004**, *428*, 736−738.

(19) Klein, C. Some Precambrian banded iron-formations (BIFs) from around the world: Their age, geologic setting, mineralogy, metamorphism, geochemistry, and origin. *Am. Mineral* **2005**, *90*, 1473−1499.

(20) Kim, J. D.; Yee, N.; Nanda, V.; Falkowski, P. G. Anoxic photochemical oxidation of siderite generates molecular hydrogen and iron oxides. *Proc. Natl. Acad. Sci. USA* **2013**, *110*, 10073−10077.

(21) Tomkinson, T.; Lee, M. R.; Mark, D. F.; Smith, C. L. Sequestration of Martian CO_2 by mineral carbonation. *Nat. Commun.* **2013**, *4*, 1−6.

(22) McCollom, T. M. Formation of meteorite hydrocarbons from thermal decomposition of siderite ($FeCO_3$). *Geochim. Cosmochim. Acta* **2003**, *67*, 311−317.

(23) Milesi, V.; Prinzhofer, A.; Guyot, F.; Benedetti, M.; Rodrigues, R. Contribution of siderite−water interaction for the unconventional generation of hydrocarbon gases in the Solimoes basin, north-west Brazil. *Mar. Pet. Geol.* **2016**, *71*, 168−182.

(24) Marocchi, M.; Bureau, H.; Fiquet, G.; Guyot, F. In-situ monitoring of the formation of carbon compounds during the dissolution of iron (II) carbonate (siderite). *Chem. Geol.* **2011**, *290*, 145−155.
(25) Milesi, V.; Guyot, F.; Brunet, F.; Richard, L.; Recham, N.; Benedetti, M.; Dairou, J.; Prinzhofer, A. Formation of CO_2, H_2 and condensed carbon from siderite dissolution in the 200-300 °C range and at 50 MPa. *Geochim. Cosmochim. Acta* **2015**, *154*, 201−211.
(26) Taran, Y. A.; Varley, N. R.; Inguaggiato, S.; Cienfuegos, E. Geochemistry of H_2- and CH_4- enriched hydrothermal fluids of Socorro Island, Revillagigedo Archipelago, Mexico. Evidence for serpentinization and abiogenic methane. *Geofluids* **2010**, *10*, 542−555.
(27) Mayhew, L. E.; Ellison, E. T.; McCollom, T. M.; Trainor, T. P.; Templeton, A. S. 2013. Hydrogen generation from low-temperature water-rock reactions. *Nature* **2013**, *6*, 478−484.
(28) Wang, Q. T.; Lu, H.; Shen, C. C.; Liu, J. Z.; Peng, P. A.; Hsu, C. S. Impact of inorganically bound sulfur on late shale gas generation. *Energy Fuels* **2014**, *28*, 785−793.
(29) Mukhina, E.; Kolesnikov, A.; Kutcherov, V. The lower pT limit of deep hydrocarbon synthesis by $CaCO_3$ aqueous reduction. *Sci. Rep.* **2017**, *7*, No. 5749.
(30) Oze, C.; Jonesb, L. C.; Goldsmithc, J. I.; Rosenbauer, R. J. Differentiating biotic from abiotic methane genesis in hydrothermally active planetary surfaces. *Proc. Natl. Acad. Sci.* **2012**, *109*, 9750−9754.
(31) Zhang, S. C.; Mi, J. K.; He, K. Synthesis of hydrocarbon gases from four different carbon sources and hydrogen gas using a gold-tube system by Fischer−Tropsch method. *Chem. Geol.* **2013**, *349*−*350*, 27−35.
(32) Sleep, N. H.; Bird, D. K. Niches of the pre-photosynthetic biosphere and geologic preservation of the Earth's earliest ecology. *Geobiology* **2007**, *5*, 101−117.
(33) French, B. M.; Rosenberg, P. E. Siderite ($FeCO_3$): Thermal Decomposition in Equilibrium with Graphite. *Science* **1965**, *147*, 1283−1284.
(34) Powell, H. E. Thermal decomposition of siderite and consequent reactions. *U.S.Bur. Mines Rept. Inv.* **1965**, *6643*, 44.
(35) Takenouchi, S.; Kennedy, G. C. The binary system H_2O-CO_2 at high temperatures and pressures. *Am. J. Sci.* **1964**, *262*, 1055−1074.
(36) Berndt, M. E.; Allen, D. E.; Seyfried, W. E., Jr. Reduction of CO_2 during serpentinization of olivine at 300 °C and 500 bar. *Geology* **1996**, *24*, 351−354.
(37) Foustoukos, D. I.; Seyfried, W. E., Jr. Hydrocarbons in hydrothermal vent fluids: the role of chromium-bearing catalysts. *Science* **2004**, *304*, 1002−1005.
(38) Horita, J.; Berndt, M. E. Abiogenic methane formation and isotopic fractionation under hydrothermal conditions. *Science* **1999**, *285*, 1055−1057.
(39) Satterfield, C. N.; Hanlon, R. T.; Tung, S. E.; Zou, Z. M.; Papaefthymiou, G. C. Initial behavior of a reduced fused-magnetite catalyst in the Fischer−Tropsch synthesis. *Ind. Eng. Chem. Prod. Res. Dev.* **1986**, *25*, 401−406.
(40) Spath, P. L.; Dayton, D. C. Preliminary Screening−Technical and Economic Assessment of Synthesis Gas to Fuels and Chemicals with Emphasis on the Potential for Biomass-Derived Syngas. NREL/TP-510-34929, 2003; p. 95. https://www.nrel.gov/docs/fy04osti/34929.pdf.
(41) Etiope, G.; Sherwood Lollar, B. Abiotic methane on earth. *Rev. Geophys.* **2013**, *51*, 276−299.
(42) Wang, W.; Wang, S.; Ma, X.; Gong, J. Recent advances in catalytic hydrogenation of carbon dioxide. *Chem. Soc. Rev.* **2011**, *40*, 3703−3727.
(43) Seewald, J. S.; Zolotov, M. Y.; McCollom, T. M. Experimental investigation of single carbon compounds under hydrothermal conditions. *Geochim. Cosmochim. Acta* **2006**, *70*, 446−460.
(44) Oze, C.; Sharma, M. Have olivine, will gas: serpentinization and the abiogenic production of methane on Mars. *Geophys. Res. Lett.* **2005**, *32*, No. L10203.
(45) Etiope, G.; Schoell, M.; Hosgormez, H. Abiotic methane flux from the Chimaera seep and Tekirova ophiolites (Turkey): understanding gas exhalation from low temperature serpentinization and implications for Mars. *Earth Planet. Sci. Lett.* **2011**, *310*, 96−104.
(46) Taran, Y. A.; Kliger, G. A.; Sevastianov, V. S. Carbon isotope effects in the open-system Fischer−Tropsch synthesis. *Geochim. Cosmochim. Acta* **2007**, *71*, 4474−4487.
(47) Smutek, M. On the Mechanism of the Chain Growth in Fischer−Tropsch Synthesis. *J. Mol. Catal.* **1984**, *24*, 257−260.
(48) van Santen, R. A.; Markvoort, A. J. Chain Growth by CO Insertion in the Fischer−Tropsch Reaction. *ChemCatChem* **2013**, *5*, 3384−3397.
(49) Pichler, H.; Schulz, H. Neuere Erkenntnisse auf dem Gebiet der Synthese von Kohlenwasserstoffen aus CO und H_2 (New insights in the area of the synthesis of hydrocarbons from CO and H_2). *Chem. Ing. Tech.* **1970**, *42*, 1162−1174.
(50) Konn, C.; Charlou, J. L.; Holm, N. G.; Mousis, O. The production of methane, hydrogen, and organic compounds in ultramafic-hosted hydrothermal vents of the mid-Atlantic ridge. *Astrobiology* **2015**, *15*, 381−399.
(51) McDermott, J. M.; Seewald, J. S.; German, C. R.; Sylva, S. P. Pathways for abiotic organic synthesis at submarine hydrothermal fields. *Proc. Natl. Acad. Sci. USA* **2015**, *112*, 7668−7672.

https://doi.org/10.1021/acs.energyfuels.1c01323
Energy Fuels 2021, 35, 11909−11919